Bistable, Pneumatically Actuated Microgripper Fabricated Using Two-Photon Polymerization and Oxygen Plasma Etching

Maura Power, Antoine Barbot, Florent Seichepine,* and Guang-Zhong Yang

Fabrication of actuatable micromechanisms onto the tip of submillimeter medical instruments permits microsurgery, cellular-level intervention, targeted drug delivery, or placement of microimplants. In these systems, a common lack of integrated microsensors or optical feedback prohibits stabilizing closed-loop control. Moreover, the low stiffness of compact actuator and microfabrication limitations lead to difficult control. Herein, a compact bistable open-loop micromechanism mounted on a small (170 μm) capillary fiber is developed. Bistabillity is utilized to control the mechanism to precise positions without the need for feedback or continuous control. Repeatable fabrication of this compact and high-resolution bistable micromechanism is achieved with a two-photon polymerization (2PP) process refined by oxygen plasma etching (OPE) that results in minimal feature size of a few hundred nanometers along the direction of the laser's axis, allowing 2PP bistable mechanisms to be fabricated in arbitrary orientations not restricted by printing direction. Finite element method simulations and experimental studies of the OPE effect are presented and used to optimize the micromechanism's bistable behavior. Finally, the feasibility of such compact bistable mechanism with a gripper that captures 50 μm spheres and passively maintains grasping without constant driving force even in long open-close cycles is demonstrated.

1. Introduction

Handling and interacting with micro-objects dynamically in vivo could support the development of new treatment and therapy paradigms such as single-cell manipulation, neuron-level implant interfacing, and micro-endovascular interventions.[1] To reach this goal, research has been carried out on the development of compact tools—those with an actuation range comparable to the size of micro-targets in vivo with multiple degrees of freedom (DOF) to facilitate manipulation within tight workspaces. Such microrobotic grippers have been proposed by using either untethered robots or as remotely controlled agents that can swim or crawl to their target.[2,3] Comparatively fewer tethered approaches—whereby the gripper has a physical connection to its power supply and controller—have also been investigated.[4–6]

Such tethered microactuators are typically fabricated using well-established micro-electrical and mechanical system (MEMS) solutions. Most of these structures use compliant flexures to leverage larger displacements by using amplifying mechanisms.[7] With compliant mechanisms, the relative motion between parts is not achieved with interlocking hinges or gears but by using thin flexural features (which will be referred to as "flexures" throughout the remainder of this article). Compliant designs are generally appealing due to their lack of friction or backlash,[8] and are particularly suitable at microscales because assembling can be challenging as scale reduces.[9,10]

A drawback of compliant gripper designs fabricated using MEMS techniques is that the overall footprint of such designs is usually much larger than the dimensions of the intended target object, leading to noncompact mechanisms. For example, in ref. [11], which has a relatively low tool-to-target size ratio, the maximum target object diameter is 7 μm and the overall gripper

M. Power, F. Seichepine
Hamlyn Centre
Imperial College London
SW7 2AZ London, UK
E-mail: f.seichepine@imperial.ac.uk

The ORCID identification number(s) for the author(s) of this article can be found under https://doi.org/10.1002/aisy.202200121.

A. Barbot
AS2M
Femto-St
25000 Besançon, France

G.-Z. Yang
Institute of Medical Robotics
Shanghai Jiao Tong University
Shanghai, China

**ADVANCED
SCIENCE NEWS**
www.advancedsciencenews.com

**ADVANCED
INTELLIGENT
SYSTEMS**
Open Access
www.advintellsyst.com

volume (including only the moving part of the mechanism, excluding the electronics) is $650 \times 150 \times 20 \mu m$. Other representative examples[5,12] have an even larger tool-to-target size ratio with mechanism dimensions on the scale of millimeters. Noncompact mechanisms may be more limited in their potential applications due to restricted access to a target object or anatomy. An alternative means of actuation for compliant mechanisms is fluidic actuation, which operates based on changes in the pressure or flow rate of liquids or gases to initiate the movement of mechanical parts. Such an approach facilitates compact and high power density at microscales.[13,14] Furthermore, both hydraulic and pneumatic approaches can be well-suited to biological applications by using a biocompatible actuation fluid such as water, saline, air, nitrogen, or oxygen.

To ensure mechanism compactness while also satisfying the constraints inherent to monolithic fabrication processes, one possible approach is to reduce the mechanism stiffness. This has been demonstrated with both untethered passive[15] and tethered active[16,17] structures using low Young's modulus materials. Thinner flexures in specific locations of 3D 2PP-printed designs were also used in our previous work for passive[18] as well as active[19] micro-mechanisms to achieve compact microtools. However, as stiffness reduces, external interactions and perturbations have a greater impact on the position and configuration of the mechanism. It is, therefore, challenging to maintain a tool's stable position setpoint without any feedback while interacting with its environment. This is a problem shared with the field of soft robotics[20]—a field that could be considered the macroscale counterpart of compliant micro-mechanisms. Moreover, static control of microscale devices can be problematic due to the inherent instability of motion at the microscale caused by, for example, mechanical noise and vibration. To avoid the need for continuous closed-loop control or constant application of forces, mechanisms with multiple discrete stable states can be used instead.

In this article, we propose a repeatable compliant and compact microactuator using a bistable mechanism that can stably occupy a pair of predefined positions. As a result, no position or state feedback is necessary to precisely reach the bistable configurations defined during the mechanism's design stage. Such behavior is possible because the flexures of compliant mechanisms store potential energy as they deform. The mechanism is in a stable configuration (i.e., a configuration that does not require a holding force) when the net stored energy of the system is at a local minimum—this state is called "stable equilibrium."

A bistable mechanism's ability to occupy different discrete positions without constant power input is desirable in many applications, such as in switches, relays,[21] or nonexplosive release mechanisms.[22] Bistable mechanisms have already been explored at the microscale, with classical MEMS fabrication method for open loop actuator[23] but also more recently using 2PP with in-plane mechanism actuated by acoustic-flow-induced force[24] or microscale logic gates actuated using optical tweezers.[25] Bistable mechanisms have also been used in macroscale pneumatic actuators for soft robotics. For example,[26] demonstrates a gripper with a latching capability that requires neither power consumption nor closed-loop control at its equilibrium states.

2PP is an effective tool to realize such a structure at the microscale because it can fabricate complex, monolithic, 3D designs with sub-micrometer precision. However, as is described in detail in the following sections of this article, to achieve bistability it was necessary to achieve feature sizes on the order of a few hundred micrometers along the axis of the 2PP laser. Due to the inherent limitations of the focused laser spot size and shape, the minimal feature size of the commercial 2PP system is just below 1 μm along the axis of the laser beam. Therefore, decreasing the feature size was essential to achieve bistable mechanisms with flexures in arbitrary 3D orientations. Combining 2PP with OPE has been used previously to reduce the minimal feature size and help design overhang microstructures with a thin support lattice etched after development.[27] We developed and describe in this article a process that combines 2PP and OPE to reach the necessary feature size along the 2PP laser axis.

Finally, we achieved a 2PP-printed pneumatically actuated micro-gripper on the distal end of a hollow-channel fiber that is capable of bistable latching open or closed. The bistable mechanism is integrated with gripper fingers that, together, are specifically designed to manipulate the chosen 50 μm diameter spherical target object. The fabrication process and principles of the proposed bistable gripper, which is approximately 100 μm across, is illustrated in **Figure 1** at the key stages of fabrication and testing: a) after 2PP printing and before OPE; b) after OPE and open; c) after OPE and closed.

2. Methods

A bistable mechanism is a mechanism that can occupy two positions in stable equilibrium and does not need a holding force to keep it in either one. An input stimulus/force is required only to "snap through" between these two states. **Figure 2**a illustrates a typical force–displacement and potential energy–displacement plot of a bistable mechanism. The two stables states can be seen to exist at the two local minima of the energy–displacement curve. The chevron-style bistable design used in this work is based on a design that forms the basis of several other previous examples of macroscale bistable mechanisms.[22,28–31] In some of these examples, two beams were stacked one on top of the other. In this work, the mechanism is fabricated at the microscale and two beams are rotated orthogonal to one another, overlapping at the shuttle which acts as the piston of the pneumatic actuation mechanism. The double-beam design is shown in Figure 2b, looking at half of the chevron bistable mechanism it is illustrated at both its first and second stable positions in Figure 2c. The parameters of the bistable unit are given herein, five of which were considered variables during preliminary tuning. A linear translation along one axis only was desired, and so all of the beams were oriented to travel along the Z-axis. The mechanism converts a linear translation of the central shuttle (or "palm") of the gripper into a rotation of the gripper fingers.

The two primary constraints that were considered for the device design were: 1) the maximum printing volume of the commercial 2PP system's galvanic mirror with its high-resolution objective lens (63x objective, NA 1.4); and 2) the choice of hollow-core fiber with a finite range of available inner-diameter (ID) and outer-diameter (OD) combinations from a commercial
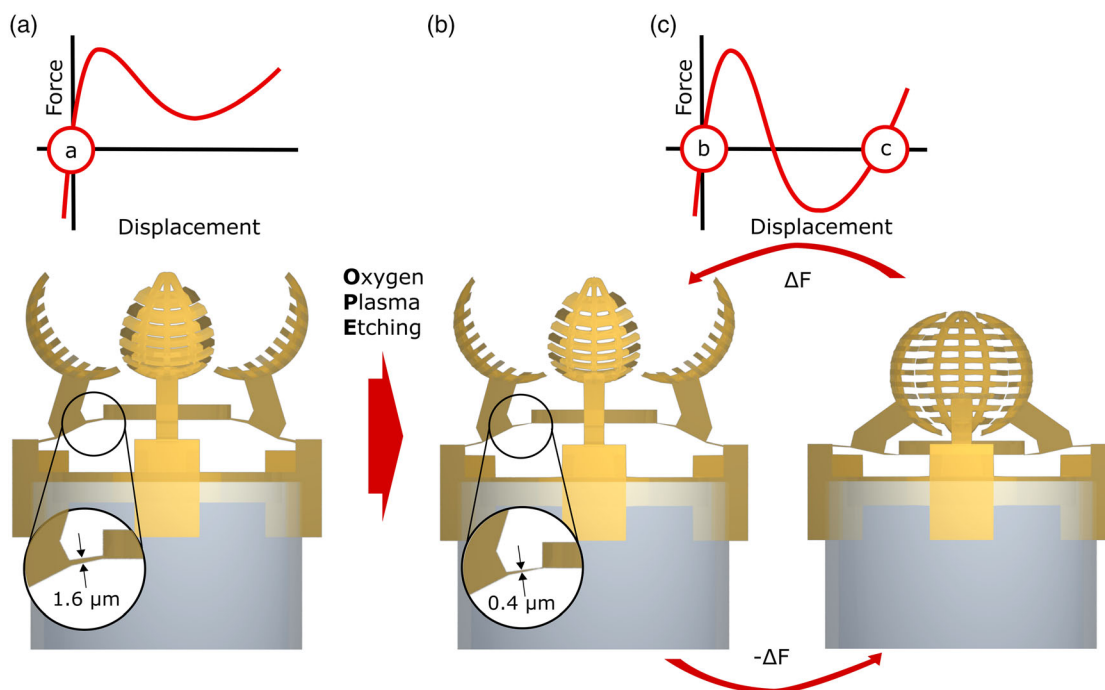
**ADVANCED
SCIENCE NEWS**
www.advancedsciencenews.com

**ADVANCED
INTELLIGENT
SYSTEMS**
www.advintellsyst.com

Figure 1. Schematic of the proposed design and operation of the bistable microgripper which is fabricated using a combination of two-photon polymerization (2PP) and oxygen plasma etching (OPE). a) The device has just one stable position directly after 2PP printing but, after etching, the gripper has two stable positions: b) the open position and c) the closed position. Transitioning between the two stable positions is achieved by applying a temporary force to the central, horizontal shuttle plate of the gripper. The flexure thickness annotated in (a,c) are representative of typical dimensions before OPE and after approximately ≈2.5 h of OPE.

supplier. The maximum printing volume, without stitching multiple different separately-printed parts together, is roughly a cube with 170 µm long sides. Structures larger than this volume need to be divided into sub-volumes within these constraints and are printed one-by-one, moving the 2PP stage between each step. This results in seams between the individual volumes. In this work, 3D volume stitching was avoided to circumvent the added fabrication complexity and structural discontinuity that would result. With this maximum diameter constraint of 170 µm, a capillary fiber with a combination of ID equal to 100 µm and OD equal to 140 µm (with cladding removed) was chosen. Another constraint to consider was the size of the target object. For this work, spheres with a diameter of 50 µm were chosen which are representative of the target applications of cellular-level manipulations.

For the bistable mechanism used in this work, the key geometric parameters are labeled in Figure 2. The width, length, and angle of the thin flexures are denoted w_h, L_h, and θ_h, respectively, and b) and the width, length, and angle of the rigid links joining the flexures are denoted w_j, L_j, and θ_j. Since the bistable mechanism is to be used as a gripper, the primary variable of interest is the change in the angle of the rigid links onto which the gripper fingers will be attached. This change in angle is denoted $\Delta\theta_g$ in Figure 2b. Since the fingers of the grippers are rigidly attached to these links, $\Delta\theta_g$ is the same for the links as it is for the gripper fingers.

With the 2PP system printing volume constraints, dimensions of the hollow-fiber substrate, and bistable mechanism principles established, the goal of the design was to incorporate these into a mechanism that: 1) fits within the various geometric constraints; 2) is capable of snap-through to a second stable state; 3) can reliably capture a target object. The final design is shown in Figure 2d and the bistable elements are highlighted in red. As stated earlier, the chosen target object was a 50 µm sphere and so the shape of gripper fingers was designed such that they close together to form a space just the right size to fit this specific object. Due to the strength of 2PP as a 3D printing technique, the shapes and sizes of the gripper fingers are easily adapted to close around target objects of different shapes and sizes.

FEM simulations were used to inform the choice of the geometric parameters of the bistable mechanism listed earlier. The 3D models, which were designed in Solidworks, were used both for mechanical simulation in Ansys and for fabrication. Ansys Workbench 2019 R1 was used and the analysis was carried out as a static structural analysis using the "Mechanical APDL" solver (see Figure S4, Supporting Information). The Young's modulus of the cured photopolymer used by the 2PP process was set to 2.5 GPa and its Poisson's ratio was set to 0.4, based on previous studies.[32,33] The underside of the anchors of the 3D model were defined as fixed supports, a displacement was applied to the central shuttle in 0.5 µm steps ranging from 0 to 14 µm and the force was derived from the reaction force on the fixed supports. The simulations showed that, for the size of the bistable gripper defined in this work, the condition for the hinge thicknesses was to be below 1 µm to achieve bistability, as shown in Figure 2e. FEM analysis was also used to verify that

ADVANCED
SCIENCE NEWS
www.advancedsciencenews.com

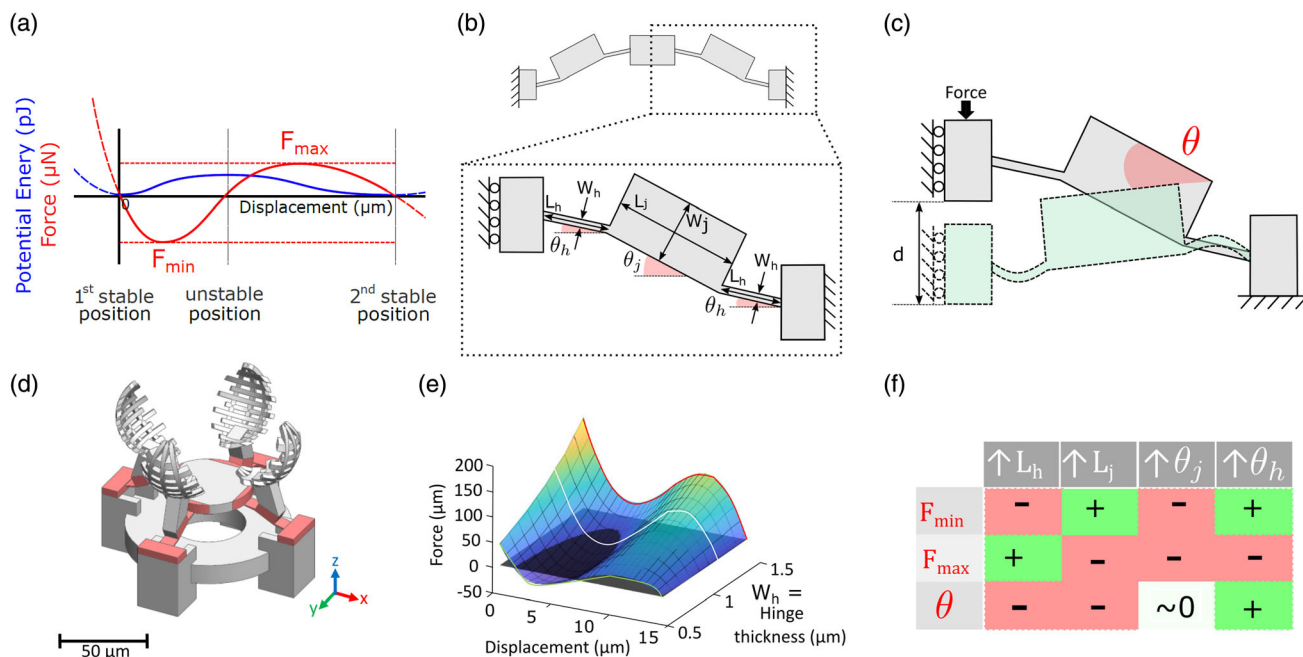ADVANCED
INTELLIGENT
SYSTEMS
www.advintellsyst.com

Figure 2. Device design and simulation of the proposed micro-gripper. a) Typical force– and energy–displacement plots for a bistable mechanism. b) Schematic of chevron bistable mechanism and a close-up of one half of the chevron mechanism labeled with key geometric parameters. c) Schematic of the two stable states of half of the chevron bistable mechanism with the change in the angle of the links and the gripper fingers (θ_g) between the two stable states annotated. d) Illustration of the bistable gripper CAD model with the flexure elements highlighted in red. The Z-axis denotes the central axis of the 2PP system's laser. e) Force–displacement curves from simulated bistable mechanisms with changing of hinge thickness. Bistable behavior is achieved when the flexure thickness is below $\approx$2.5 µm. f) Colormap illustrating the relative change in the peak force and the angular difference (θ) by varying several geometric parameters of the structure. White denotes no change, green denotes a positive change and red denotes a negative change. The geometric parameters of the bistable mechanism L_h, L_j, θ_h, θ_j are annotated in (b), θ_g in (c), and F_{min} and F_{max} in (a).

the final design would be possible to actuate with the range of pressure differentials capable of being produced with the available laboratory setup. The effects of varying the mechanism's geometric parameters on the force profile are described in further detail in the Supporting Information. The final chosen parameters for the gripper CAD model were are follows: $w_h = 1$ µm, $L_h = 8$ µm, $\theta_h = 12°$, $w_j = 8$ µm, $L_j = 16$ µm, and $\theta_j = 27°$.

2PP relies on the local curing of a liquid photopolymer by a focused laser which results in an ellipsoid voxel of hardened material. In the case of the commercial setup Photonic Professional GT2 (Nanoscribe GmbH, Karlsruhe, Germany), the typical highest resolution dimensions of a single voxel can be described by an ellipsoid with a cross-sectional diameter of 0.3 µm in the XY plane width and a height of 0.8 µm along the Z-axis. In practice, when printing 3D models it is necessary to overlap voxels between layers, and it was found the flexures' minimum achievable thickness was closer to µm. Thus, the resolution required to achieve the desired bistable mechanism behavior for the proposed design cannot be achieved with 2PP technology alone. OPE has been shown to allow for the fabrication of thinner structures and could be used to achieve the desired mechanical behavior. As the final geometry of the devices is one of the key parameters, good control over the OPE process is necessary for the reliable fabrication of the bistable mechanism presented in this article.

Flexible elements are the building blocks of compliant mechanisms, which act as approximations to hinges i.e., points about which the mechanism bends or rotates. Typically, in compliant designs, thicker areas of the mechanism undergo relatively negligible deformation compared to flexures. To print a small bistable mechanisms (i.e., similar in scale to the mechanisms in this work) using 2PP, there are a number of challenges. The first is that the flexures in the bistable mechanism need to be thin; typically a few hundreds of nanometers. By its nature, 2PP has a different minimum feature size in the XY plane compared to its Z-axis (along the laser axis), as denoted in the coordinate frame in Figure 2d. When considering structures with feature sizes close to the limitations of 2PP's resolution, the orientation of the structure to be printed relative to the 2PP system's laser Z-axis axis needs to be considered. However, in many cases, the orientation of printing is dictated by the fact that the flat surface of the substrate needs to be orthogonal to the Z-axis. In this work, the thickness of the thinnest feature of interest—the flexures—is dictated by the Z-axis resolution. This means that the flexures can be printed with a minimal thickness of around 1–1.5 µm. Furthermore, printing extremely thin features can be problematic during the development phase of 2PP polymerization during which the mechanisms are exposed to high capillary forces by the solvent as it evaporates during post-development causing low yields and poor repeatability.[34] OPE allows for a stronger structure to be printed initially, with the ability to reduce the

**ADVANCED
SCIENCE NEWS**

www.advancedsciencenews.com

**ADVANCED
INTELLIGENT
SYSTEMS**
Open Access

www.advintellsyst.com

dimensions post-development. Our chosen approach is, therefore, to print flexures with a nominal thickness of 1 μm and to add a plasma post-processing step to reduce this thickness to a few hundred of nanometers.

OPE was used to partially remove a thin outer layer of the fully printed micro-gripper in an isotropic manner and, as a result, fine-tune the bistable behavior of the mechanism. The rate of OPE (R_{OPE}) needs to be known to allow OPE to be used as a precise fabrication step. Experiments were conducted to determine the R_{OPE} and to understand its relationship to the laser dose used during the 2PP process. Variable laser dose has been shown to affect many material properties of 2PP structures, however, the relationship between laser dose and the etch rate has not been reported in the literature to date, to the authors' knowledge.

Thin, cylindrical beams printed using 2PP were used to characterize the etch rate (R_{OPE}) of the photoresist as a function of 2PP laser printing power and to characterize the stiffness of the beams (as flexures) as a function of 2PP laser power and etch time. The OPE depth (d_{OPE}) of a flexure after t minutes of etching, is defined by

$$d_{OPE} = D_{T=0} - D_{T=t} \tag{1}$$

where $D_{T=0}$ is the beam diameter before OPE and $D_{T=t}$ is the diameter after t minutes of OPE. The etch rate accounts for material removal on both exposed sides of the beam diameter—this is the case for the flexures in the bistable mechanisms that are the target feature for reduction by OPE. As an aside, in the case where a structure is attached to a substrate, etching will occur only on the exposed surface and so the d_{OPE} would be half of the value defined earlier. The R_{OPE} (reported in nanometers per minute in this article) is defined by

$$R_{OPE} = \frac{d_{OPE}}{t} \tag{2}$$

where d_{OPE} is the etch depth in nanometers and t is the duration of the OPE session in minutes. To characterize R_{OPE}, test beams were designed to have a circular cross-sectional diameter (D) of 2 μm and a length of 20 μm. The beams were flared at the end to allow a point of contact for force–displacement experiments. This value for D was chosen as it was close to the flexure width in the final bistable gripper design. Sets of test beams were printed to include 7 different laser powers, ranging from 7.5 to 22.5 mW in steps of 2.5 mW. However, the 7.5 mW beams did not support themselves, and therefore were not included in the final testing and analysis. Two different sets of beams were printed separately for R_{OPE} and force study. The groups of test beams are illustrated further in the Supporting Information. The 2PP printing power (P) was varied to assess how much the degree of polymerization of the photoresist affects the plasma etch rate. The other primary printing parameters (laser speed, line spacing, and hatching distances) were kept constant throughout this work. After omitting the 7.5 mW beams, this resulted in a total of 126 beam measurements. The plasma treatment parameters were kept constant across all experiments using a 200 W plasma oven working at 40 kHz and an oxygen pressure of 0.15 mBar. Each flexure beam was imaged under a scanning electron microscope (SEM) directly after printing ($T = 0$ min of OPE), and then at $T = 30$, 60, 90, and 120 min of OPE. This provided a direct comparison

between 1) individual beams at various stages of etching; 2) similar beams printed and etched under similar conditions. **Figure 3**a shows the same beam overlaid and color-coded at each of the 5 stages of OPE, and the source images as given the Figure S3, Supporting Information. A custom image processing algorithm, using Python's OpenCV library, was used to automatically measure the beam thicknesses across the dataset. The results were used to determine the post-OPE diameter as a function of printing power and etching time and, from this, the R_{OPE}. The primarily observed trends are discussed and summarized in the following paragraphs.

The beam diameters immediately after 2PP printing/before OPE were found—as expected—to vary slightly as a function of printing power. The diameter was specified as 2 μm in diameter in the CAD model, but in practice, this ranged linearly from a mean of 1.71 to 1.97 μm for laser powers ranging from 10 to 22.5 mW, respectively. This trend is shown by the top row of blue boxplots in Figure 3b. This variation arises due to a combination of the polymerized voxel size and shrinkage during development[35] and, given that the highest resolution voxel width of 0.3 μm is an appreciable fraction of the desired width of 2 μm. Therefore, the variation of beam diameter with laser power is particularly pronounced for such thin structures and, therefore, the same was expected for the bistable mechanisms of thin flexures.

The mean R_{OPE} was found to vary somewhat between the four distinct 30 min OPE sessions but, for a given session, the etch rate was quite consistent regardless of laser power. This can be seen in the constant offset between the 5 trend lines in 3b. For the first 30 min of the session, the average change in the beam diameter was 0.38 ± 0.03 μm, for the second 30 min of the session, it was 0.31 ± 0.02 μm, for the third it was 0.39 ± 0.02 μm and for the last session, it was 0.31 ± 0.03 μm. This gives an average value of $R_{OPE} = 11.6 \pm 0.8$ nm min^{-1}.

To characterize the stiffness change caused by reducing the beam dimension with OPE, another 3 sets of test beams was fabricated using the same printing and etching conditions described earlier. Again, the lowest power samples (7.5 mW) were not included in the final analysis. Each beam was deflected between 1 and 2 μm (Figure 3c), and the corresponding stiffness measurements (calculated by dividing the force by displacement) are plotted in Figure 3d. As expected, reducing the diameter of the flexure beams significantly reduces the stiffness of the beam because the cylindrical beam stiffness is inversely proportional to the fourth power of the beam diameter. The data used for this plot was only taken from beam measurements whose force readings were discernibly above the noise floor of the force sensor.

The results of these preliminary investigations summarized earlier indicated that OPE could indeed help to fine-tune the force–displacement behavior of 2PP-printed bistable mechanisms. In particular, this approach is useful for compliant mechanisms that are already at the limit of 2PP's spatial resolution limits.

3. Results

The fabrication of the proposed device followed a similar process to that described in previous work on passive, compliant grippers
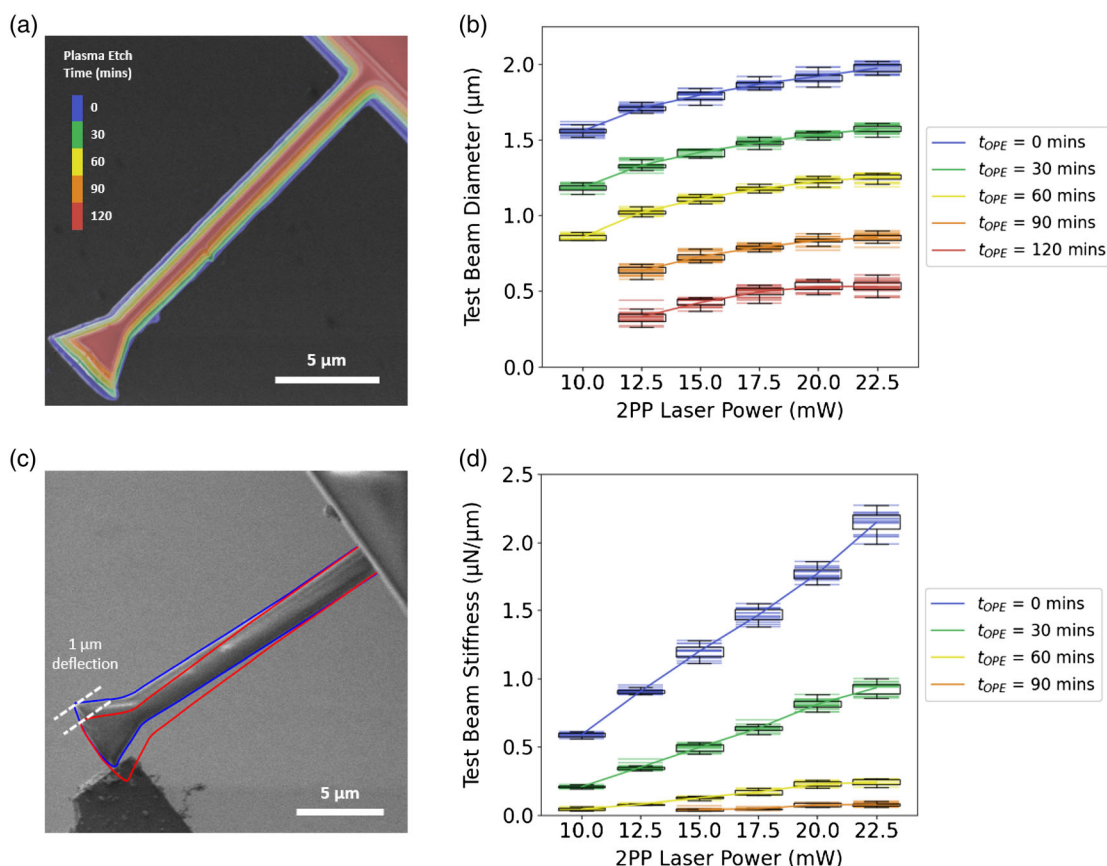
Figure 3. Characterization of the effects of OPE on IP-Dip photoresist as a function of time and laser printing power on a 2 μm diameter test beam. a) Scanning electron microscope (SEM) image stack of a beam printed with 12.5 mW laser power after 0, 30, 60, 90, and 120 min of OPE. Scale bar 5 μm. b) Plot of beam thicknesses after 0, 30, 60, 90, and 120 min of OPE for beam printed with a laser power of 10, 12.5, 15, 17.5, 20, and 22.5 mW. Each box plot captures the results of 21 data points acquired from image sets such as that shown in (a). This plot shows that the median beam thickness is linearly dependent on the printing power, and that the etch rate is primarily time-dependent (and not a function of printing power). c) SEM images of a beam printed with 12.5 mW laser power being bent with a force sensor by 1 μm. d) Plot of the test beam stiffness (i.e., force in μN required per 1 μm of displacement) for the test beam design shown in (a).

printed onto optical fibers.[6] Compared to fabricating onto a solid optical fiber substrate, the hollow channel fibers added some more complexity to the fabrication and development process by allowing the viscous photoresist to climb up the inner channel behind the printed structure. This resin was difficult to fully flush out during the development process if it went sufficiently deep into the channel. To minimize this capillary action, epoxy resin was used to plug the opposite end of the hollow fiber.

The 2PP printing parameters for the bistable gripper were as follows: a slicing distance of 0.3 μm, a hatching distance of 0.2 μm, a laser scan speed of $10,000$ μm s^{-1}, and laser printing powers of 15 mW. After 2PP printing, the flexures of the bistable mechanism were reduced from a starting thickness of ≈1.6 μm to a few hundred nanometers using OPE, at which point reliable bistability could be achieved. It was found that it would take about 120–150 min of plasma etching using the same settings as used for the test beam R_{OPE} analysis described earlier. An illustrative example of a sample bistable gripper that was etched for 145 min is given in Figure S9, Supporting Information. After 145 min of OPE, the resulting hinge thickness reduction (d_{OPE}) is 1.35 μm.

This corresponds to a R_{OPE} of 9.3 nm min^{-1} which falls just outside the lower bound of the range of the etch rate 11.6 ± 0.8 nm min^{-1} reported in the previous section. We believe that the process variation, evident in this work and other similar published work from academic microfabrication facilities, is within reasonable limits of experimental and fabrication error. Further analysis with larger sample sets could be conducted in the future to derive more statistically significant R_{OPE} results that take into account fabrication variation that arises as a result of both 2PP and OPE.

Pneumatic actuation in the air was chosen as the source of power to drive the microscale devices presented in this article. When scaling down, surface forces (such as pneumatic forces) are proportional to the square of the dimension being scaled, whereas volumetric forces (such as magnetic forces) are proportional to the cube of the dimensions. As a result, sufficiently large forces for actuation can be achieved relatively easily with hydraulic and pneumatic approaches. Moreover, compared to other driving techniques, no significant side-effects, such as heating or strong electric field, which are undesirable for certain biological applications, are produced at the actuation point.

**ADVANCED
SCIENCE NEWS**

www.advancedsciencenews.com

**ADVANCED
INTELLIGENT
SYSTEMS**
Open Access

www.advintellsyst.com

Figure 4a shows two SEM images of the same bistable gripper both in its open and closed states. The gripper was fabricated in its open state (at the distal end of the capillary tube) and subsequently imaged in the SEM. Next, the gripper was removed from the SEM and the proximal end of the capillary was connected to the negative pressure source, which applies a "pulling" force on the central shuttle of the gripper to close it. After the gripper was switched to its closed state of equilibrium, the capillary tube was disconnected from the pump and placed back inside the SEM to take the image shown on the right of Figure 4a. This experiment illustrates that the bistable device is robust to the disturbances involved in operations such as connecting/disconnecting the pressure source, transporting the device to/from the SEM, and placing it into a vacuum.

The pressures required to open and close the gripper were tested experimentally. Figure 4c shows 11 cyclic open and closing pressures that were recorded for 3 different devices prepared with identical fabrication steps. Although there is a clear variation in pressures required to toggle between states for each device, the change in pressure required to actuate a given mechanism varies comparatively little over the measurement period shown. The lifespan of a selection of mechanisms was also tested by repeated switching between the open and closed states over a longer period of time until failure. Over these longer periods of sustained toggling, the switching pressure was seen to drift

somewhat, which was likely due to the viscoelastic properties of the photoresist. Figure 4d shows the profile of the one complete pressure cycle that was used for lifetime testing. The profile consisted of fast and slow changes of pressure: fast where the bistable mechanism was not expected to change state, and slower when close to the snap-through pressures. This allowed for a more precise estimation of the snap-through pressures. Device-dependent variation in the toggling lifetime was observed. In some cases, there were just a few cycles before catastrophic failure, and in several other cases, the mechanisms could operate over 100 cycles without breaking. This variation between structures underlines that there was still a degree of fabrication variation that remains to be understood and controlled in future work. A video of two different grippers toggling over 100 times each is provided in the Supporting Information.

As a final validation experiment of the bistable gripper was conducted—a grasping task was performed to demonstrate the gripper's ability to stably capture and release spherical targets. The gripper is mounted on top of a piezoelectric micro-positioning robot (miBot, Imina Technologies) which provides 4 degrees of freedom. **Figure 5**a illustrates the experimental setup, with a close-up rendering of the grasper approaching a target object in 5b. The steps of the grasping task are shown in Figure 5c, from left to right: first, the manipulator-mounted pneumatic gripper approached the substrate upon which the
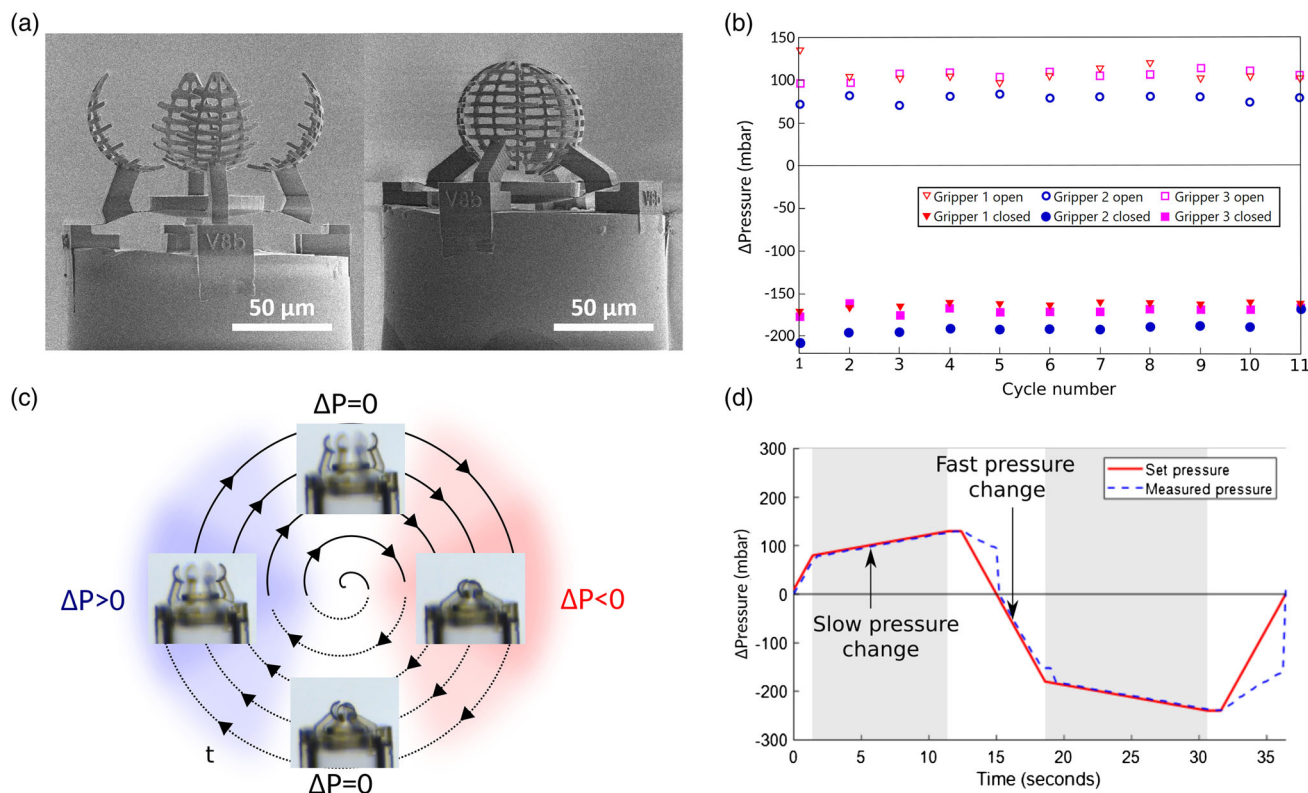

Figure 4. Experimental validation of device behavior and characterization: a) SEM images of a bistable gripper in both stable states with no holding force. b) Plot of pressures required to transition cyclically between states for 3 different bistable grippers. c) Illustration of a prototype bistable micro-gripper (see additional pictures of the gripper in Figure S7, Supporting Information). d) Force profile used for lifetime testing. The profile consists of fast and slow regions: fast where the mechanism is not expected to change states, and slow when higher precision is required to determine the point at which the mechanism changes state.
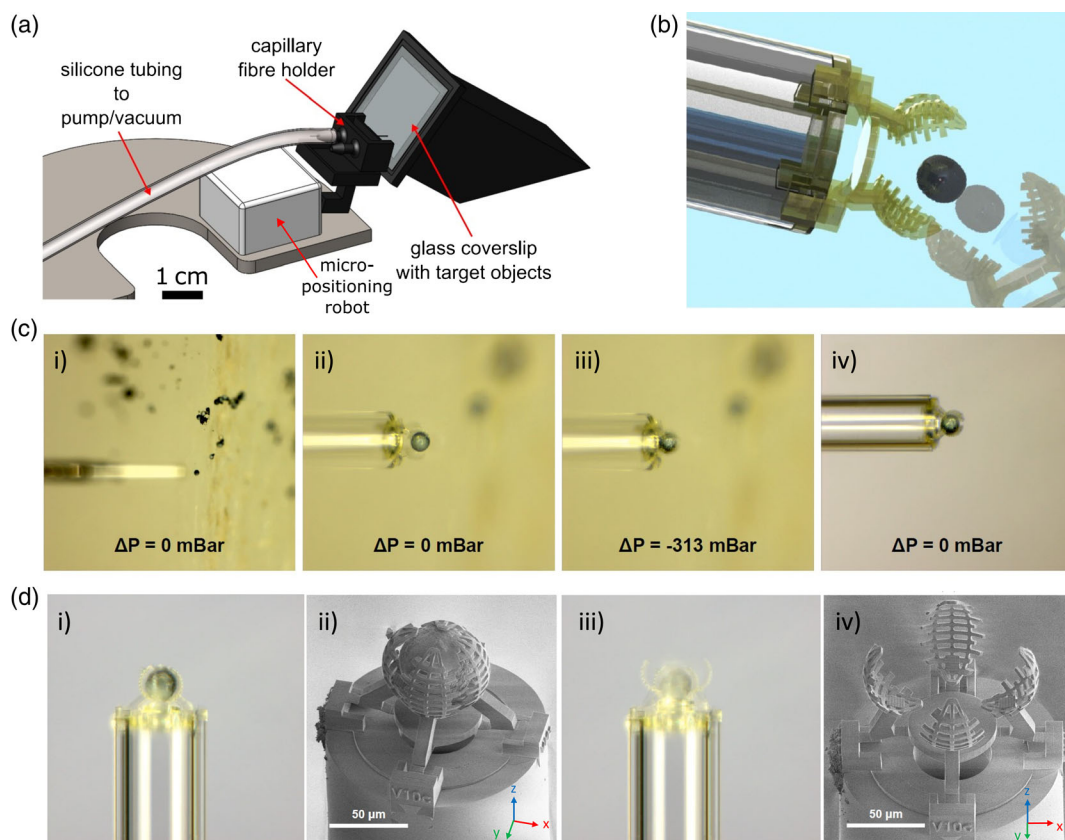
**ADVANCED
SCIENCE NEWS**

www.advancedsciencenews.com

**ADVANCED
INTELLIGENT
SYSTEMS**
Open Access

www.advintellsyst.com

Figure 5. Grasping and release task with the bistable gripper mechanism in air. a) Experimental setup under a microscope with a micro-positioning robot, tubing to microfluidic pressure generators, and bistable gripper on hollow-core fiber. b) Illustration of the gripper approaching a target object (a 50 μm glass sphere). c) Series of microscope images taken during the grasping task. The air pressure differential at each step is overlaid, and the last frame shows that the pressure is not holding the bistable gripper mechanism closed. See full video in Supporting Information. d) Series of: i and iii) optical and ii and iv) SEM images taken before and after the release of the spherical object.

target spheres were placed Figure 5ci, once the gripper is close enough to the target, its fingers can be aligned around it Figure 5cii, the pump is turned on briefly to create a negative pressure differential close to the gripper Figure 5ciii and once the target is grasped the pump is turned off before retracting from the substrate Figure 5civ. To further demonstrate the stability of the gripper's closed state, the capillary fiber holder was fully disconnected from the pump, and placed inside the vacuum chamber of an SEM (Figure 5di,ii). Finally, the fiber holder was returned to the optical microscope setup, the pump was used to apply a positive pressure to release the captured particle, Figure 5diii,iv. We did not observe any disturbance on the target object from the airflow of the actuator. However, for applications where such flow would have a negative impact on the surrounding environment or to increase the gripper force we suggest incorporating a liquid seal into the design, as demonstrated in our previous work.[19]

4. Conclusions

The variable range in the lifetime of the grippers is suspected to be due primarily to fabrication variations (as was also seen in the test beams) which leads to nonuniform thickness along the length of the flexures and, therefore, weak points. This may be due to the variability in the R_{OPE} leading to the over-etching of some designs. This should be considered for further optimization toward the repeatability of the fabrication process. To compensate for the variability in the resulting flexure thicknesses in this work, bistable grippers were etched in short sessions as they approached several hundreds of nanometers in thickness and tested for bistability between these shorter fine-tuning OPE sessions.

It is important to note also that many other factors can impact the bistable performance of the design including laser dose parameters (such as slicing and hatching distances and laser speed) as well as OPE parameters (such as pressure and frequency), as discussed previously. Another important factor to consider is the internal stresses in the printed polymer material, and how these can be reduced or optimized to improve the lifetime of the tool, should repeated use be a requirement for a given application.

In designing the gripper, its dimensions were determined by a combination of factors including the size of the hollow-core fiber upon which it was being printed, the limitations of the maximum allowed 2PP printing volume without the need for 3D volume

**ADVANCED
SCIENCE NEWS**

www.advancedsciencenews.com

**ADVANCED
INTELLIGENT
SYSTEMS**
Open Access

www.advintellsyst.com

stitching and the volume of the target object for grasping. It would be feasible to print larger structures by changing the printing strategies and/or using a lower resolution lens that would facilitate larger scan diameters. Finally, using additional strategies such as a sealed version of the gripper, would allow for much larger pneumatic forces to be leveraged.[19]

2PP printing and OPE measurements showed clear trends that were consistent across the dataset. The majority of all beam thickness measurements fell within a range of $\pm 0.03\,\mu m$ of the mean, and the standard deviation was found to be $\pm 0.04\,\mu m$. Plasma etching was also found to be a very effective means of altering the stiffness of a flexure beam by way of thickness reduction. Unlike other material properties that are influenced by the laser dose, it appears from these results that there is a minimal impact on the R_{OPE} as a function of the laser power. It is possible that R_{OPE} may be affected by tuning other printing parameters that were kept constant in this work, such as 2PP line distance and/or laser scan speed and OPE gas pressure and/or source frequency.

In summary, this work has explored how to fabricate a bistable mechanism for the manipulation of objects on a scale of a few tens of micrometers. FEM simulation predicted that the resolution needed for the fabrication of the desired geometry is lower than the resolution offered by a commercial 2PP system. We explored OPE as a method to alter the 2PP structures to achieve the physical parameters required for the desired bistable behavior. In doing so, this work demonstrates that 2PP-printing of bistable mechanisms does not need to be restricted to printing in the plane orthogonal to the laser's axis, as was previously reported in the literature. This is an important point to highlight because one of 2PP's main advantages over standard MEMS technology is the ability to readily create truly 3D structures at the micrometer scale.

We showed that OPE affects the stiffness of thin flexural beams printed with IP-Dip material and 2PP by reducing their cross-sectional area. The etch rate was characterized as a function of both laser printing power and OPE time. This feature-reduction method then demonstrated how a pneumatically-actuated gripper can achieve bistable behavior.

Microscale mechanisms could greatly benefit from such multiple stability behavior and versatile fabrication techniques as 2PP. Other applications of bistable behavior can be found in micro-implants. By tuning the adhesion between the microstructure and the capillary tube, a system that detached from the capillary to remain grasp on a tissue or living organism could be designed. The bistable property would guarantee a robust grasping of the microstructure even after manipulation which could serve as useful for in vivo implantation of micro-implant. The device presented in this article is operated in the air but the 2PP fabrication process takes place in a liquid environment and is subjected to being immersed in a liquid solvent and also the evaporation of that solvent. Therefore, we are confident that only minor design optimizations would be required to adapt such a system to a wet, biological environment. While tested and submerged in water, the gripper remains operational. Supporting information S4 shows a picture of one of the grippers immersed in water and used for an actuation test in liquid. No gas entrapment was seen in this example probably due to the hydrophilicity of the 2PP material. Nevertheless, the gas bubble remaining in the structure could be further prevented by wetting the gripper first from the pneumatic tubing and adapting the design to optimize the wetting of the structure. Apart from biomedical applications, such mechanisms could also be used for micro-assembly or ultra-precision pick-and-place tasks.

We believe that this demonstration of a bistable micromechanism at the tip of a capillary fiber is an important contribution toward the fabrication of precise in situ micro-tools with different stable positions that are robust to external perturbation and possess reliable control capability.

5. Experimental Section

Fabrication of Test Flexures for 2PP and OPE Characterisation: A 2PP system (Nanoscribe) was used to 3D print the microscale hinges. The structures were printed in the dip-in configuration (i.e., resist between the glass slide and objective lens) and IP-Dip photoresist (Nanoscribe) was used. The 2PP printing parameters were as follows: slicing distance of 0.3 μm, a hatching distance of 0.2 μm, laser scan speed of 10 000 μ s^{-1}, and varying laser powers over the range that resulted in viable prints. The test set, depicted in Figure S2a, Supporting Information, comprised of 7 similar test flexures printed with the following laser powers: 7.5, 10, 12.5, 15, 17.5, 20, and 22.5 mW. Each structure was printed 7 times onto 3 indium tin oxide (ITO) coated silica glass slides. The test sets were printed at the very edge of the glass slides to allow access to the force sensor. All structures for a given test (i.e., etch rate or mechanical characterization) were printed within the same session, to minimize fabrication variation.

Fabrication of Bistable Grippers for Pneumatic Actuation: As with the test flexures, 2PP was used to print the bistable grippers using an IP-Dip photoresist. The same slicing, hatching, and laser speed parameters as described earlier were used and the laser power used was 15 mW. The hollow core, fused silica capillary tubing (TSP100170, Polymicro Technologies supplied by CM Scientific) has an inner diameter (ID) of 100 μm, a silica outer diameter (OD) of 140 μm and polyimide coating that brings the total OD to ≈170 μm. It was found that printing with concentric contours resulted in more accurate versions of the 3D models (e.g., notably less sagging) compared to printing with parallel lines.

Oxygen Plasma Etching: Etching was realized on a low-pressure plasma system (Atto, Diener) using oxygen gas, a generator power of 200 W (100% of the maximum nominal power), and a fixed frequency of 40 kHz. Gas pressure was kept constant at 0.15 mBar for all experiments. For the test flexures, each plasma etching session lasted 30 min and all sample slides were etched at the same time. For the bistable gripper, the initial plasma etching session was 2 h and then short 10–15 min sessions were used for fine-tuning to achieve bistability.

Characterization of Plasma Etch Rate: An SEM (Lyra3, Tescan) was used to acquire high-resolution images to determine the change in flexure thickness as a function of printing power and etch time. Imaging was carried out at a working distance of ≈7.6 mm and an accelerating voltage of 1 kV. For the images used to characterize the hinge thickness and deflection, a fixed magnification of 32kX was used which resulted in an image resolution of ≈8.4 nm pixel^{-1}.

Characterization of Test Flexure Stiffness: Force–displacement tests were conducted to determine the test flexure stiffness, and were carried out in an SEM using similar imaging parameters to those described earlier. A micromanipulator (MM3A-EM, Kleindiek) and force sensor (FMT-120, Kleindiek) was used to displace the hinges by a distance between 1 and 2 μm (i.e., ≤10% of the flexure length). Several pairs of force–displacement measurements were acquired for each test flexure.

Actuation of Bistable Gripper: A pair of microfluidic pressure generators (Mitos Fluika Vacuum and Pump), connected via a control valve (Mitos Fuika Control Valve, Dolomite), were used to control the air pressure/speed.

Grasping Task with Bistable Gripper: A sphere of ≈50 μm diameter (HCMSBLK-WHT 45–53 μm, Cospheric) was placed on a tilted glass slide

(at 55° with respect to the microscope imaging plane) and used as a target. A bistable gripper was mounted onto a micro-positioning robot (MiBot, Imina Technologies) for positioning of the gripper relative to the target object during the gripping task. The experimental setup is illustrated in Figure 5a.

Supporting Information

Supporting Information is available from the Wiley Online Library or from the author.

Acknowledgements

Conflict of Interest

The authors declare no conflict of interest.

Data Availability Statement

The data that support the findings of this study are available from the corresponding author upon reasonable request.

Keywords

[1] G.-Z. Yang, J. Bellingham, P. E. Dupont, P. Fischer, L. Floridi, R. Full, N. Jacobstein, V. Kumar, M. McNutt, R. Merrifield, B. J. Nelson, B. Scassellati, M. Taddeo, R. Taylor, M. Veloso, Z. L. Wang, R. Wood, *Sci. Rob.* **2018**, *3*, eaar7650.

[2] E. Diller, M. Sitti, *Adv. Funct. Mater.* **2014**, *24*, 4397.

[3] J. C. Breger, C. Yoon, R. Xiao, H. R. Kwag, M. O. Wang, J. P. Fisher, T. D. Nguyen, D. H. Gracias, *ACS Appl. Mater. Interfaces* **2015**, *7*, 3398.

[4] D. Martella, S. Nocentini, D. Nuzhdin, C. Parmeggiani, D. S. Wiersma, *Adv. Mater.* **2017**, *29*, 1704047.

[5] F. Beyeler, A. Neild, S. Oberti, D. J. Bell, Y. Sun, J. Dual, B. J. Nelson, *J. Microelectromech. Syst.* **2007**, *16*, 7.

[6] M. Power, A. J. Thompson, S. Anastasova, G. Z. Yang, *Small* **2018**, *14*, 1870069.

[7] F. Wang, C. Liang, Y. Tian, X. Zhao, D. Zhang, *IEEE/ASME Trans. Mechatron.* **2016**, *21*, 1262.

[8] L. L. Howell, *Compliant Mechanisms*, Wiley-Interscience **2001**, ISBN 978-0-471-38478-6.

[9] B. D. Jensen, L. L. Howell, L. G. Salmon, *J. Mech. Des.* **1999**, *121*, 416.

[10] S. Kota, J. Joo, Z. Li, S. M. Rodgers, J. Sniegowski, *Analog Integr. Circuits Signal Process.* **2001**, *29*, 7.

[11] N. Chronis, L. P. Lee, *J. Microelectromech. Syst.* **2005**, *14*, 857.

[12] Z. Long, J. Zhang, Y. Liu, C. Han, Y. Li, Z. Li, *IEEE Trans. Compon. Packag. Manuf. Technol.* **2017**, *7*, 2045.

[13] A. Barbot, M. Power, F. Seichepine, G.-Z. Yang, *Sci. Adv.* **2020**, *99*, 99.

[14] M. De Volder, D. Reynaerts, *J. Micromech. Microeng.* **2010**, *20*, 043001.

[15] T. Xu, J. Zhang, M. Salehizadeh, O. Onaizah, E. Diller, *Sci. Rob.* **2019**, *4*, eaav4494.

[16] J. Paek, I. Cho, J. Kim, *Sci. Rep.* **2015**, *5*, 1.

[17] H.-T. Lee, F. Seichepine, G.-Z. Yang, *Adv. Funct. Mater.* **2020**, *30*, 2002510.

[18] M. Power, A. J. Thompson, S. Anastasova, G.-Z. Yang, *Small* **2018**, *14*, 1703964.

[19] A. Barbot, M. Power, F. Seichepine, G.-Z. Yang, *Sci. Adv.* **2020**, *6*, eaba5660.

[20] A. D. Marchese, R. Tedrake, D. Rus, *Int. J. Rob. Res.* **2016**, *35*, 1000.

[21] R. A. M. Receveur, C. R. Marxer, R. Woering, V. C. M. H. Larik, N. F. de Rooij, *J. Microelectromech. Syst.* **2005**, *14*, 1089.

[22] S. A. Zirbel, K. A. Tolman, B. P. Trease, L. L. Howell, *PLoS One* **2016**, *11*, e0168218.

[23] V. Chalvet, Y. Haddab, P. Lutz, *IEEE Trans. Rob.* **2013**, *29*, 641.

[24] M. Kaynak, A. Dolev, M. S. Sakar (Preprint) arXiv:2205.12625, v1, submitted: May **2022**.

[25] Y. Song, R. M. Panas, S. Chizari, L. A. Shaw, J. A. Jackson, J. B. Hopkins, A. J. Pascall, *Nat. Commun.* **2019**, *10*, 1.

[26] P. Rothemund, A. Ainla, L. Belding, D. J. Preston, S. Kurihara, Z. Suo, G. M. Whitesides, *Sci. Rob.* **2018**, *3*, eaar7986.

[27] A. J. Gross, K. Bertoldi, *Small* **2019**, *15*, 1902370.

[28] I. H. Hwang, Y. S. Shim, J. H. Lee, *J. Micromech. Microeng.* **2003**, *13*, 948.

[29] D. A. Wang, H. T. Pham, Y. H. Hsieh, *Sens. Actuators, A* **2009**, *149*, 143.

[30] G. Chen, Y. Gou, A. Zhang, *J. Mech. Des.* **2011**, *133*, 081007.

[31] N. D. K. Tran, D. A. Wang, *Mech. Mach. Theory* **2017**, *115*, 114.

[32] J. Qu, M. Kadic, A. Naber, M. Wegener, *Sci. Rep.* **2017**, *7*, 40643.

[33] M. Kadic, T. Bückmann, N. Stenger, M. Thiel, M. Wegener, *Appl. Phys. Lett.* **2012**, *100*, 191901.

[34] A. A. Bauhofer, S. Krödel, J. Rys, O. R. Bilal, A. Constantinescu, C. Daraio, *Adv. Mater.* **2017**, *29*, 1703024.

[35] X. Zhou, Y. Hou, J. Lin, *AIP Adv.* **2015**, *5*, 030701.